Continuum of quantum fluctuations in a three-dimensional $S=1$ Heisenberg magnet

K. W. Plumb,[1] Hitesh J. Changlani,[1] A. Scheie,[1] Shu Zhang,[1] J. W. Krizan,[2] J. A. Rodriguez-Rivera,[3,4] Yiming Qiu,[3] B. Winn,[5] R. J. Cava,[2] and C. L. Broholm[1,3,6]

[1]*Institute for Quantum Matter and Department of Physics and Astronomy, The Johns Hopkins University, Baltimore, MD 21218, USA*

[2]*Department of Chemistry, Princeton University, Princeton, NJ 08544*

[3]*NIST Center for Neutron Research, National Institute of Standards and Technology, Gaithersburg, MD 20899, USA*

[4]*Department of Materials Science and Engineering, University of Maryland, College Park, MD 20742, USA*

[5]*NScD Division, Oak Ridge National Laboratory, Oak Ridge, Tennessee 37831-6473, USA*

[6]*Quantum Condensed Matter Division, Oak Ridge National Laboratory, Oak Ridge, Tennessee 37831-6473, USA*

(Dated: November 22, 2017)

Conventional crystalline magnets are characterized by symmetry breaking and normal modes of excitation called magnons with quantized angular momentum $\hbar$. Neutron scattering correspondingly features extra magnetic Bragg diffraction at low temperatures and dispersive inelastic scattering associated with single magnon creation and annihilation. Exceptions are anticipated in so-called quantum spin liquids as exemplified by the one-dimensional spin-1/2 chain which has no magnetic order and where magnons accordingly fractionalize into spinons with angular momentum $\hbar/2$. This is spectacularly revealed by a continuum of inelastic neutron scattering associated with two-spinon processes and the absence of magnetic Bragg diffraction. Here, we report evidence for these same key features of a quantum spin liquid in the three-dimensional Heisenberg antiferromagnet $NaCaNi_2F_7$. **We show that despite the complication of random Na^{1+}-Ca^{2+} charge disorder,** $NaCaNi_2F_7$ is an almost ideal realization of the spin-1 antiferromagnetic Heisenberg model on a pyrochlore lattice. Magnetic Bragg diffraction is absent and 90% of the **neutron** spectral weight forms a continuum of magnetic scattering with low energy pinch points, indicating $NaCaNi_2F_7$ is in a Coulomb-**like** phase. **Our results demonstrate that disorder can act to freeze only the lowest-energy magnetic degrees of freedom; at higher energies, a magnetic excitation continuum characteristic of fractionalized excitations persists.**

The existence of a spin liquid for isotropically interacting classical spins on the pyrochlore lattice was first proposed by Jacques Villain nearly 40 years ago.[1] Since then, it has been established that the classical ($S \to \infty$) Heisenberg antiferromagnet does not undergo any magnetic ordering transition.[2–6] The magnetic interaction energy is minimized by all spin configurations with vanishing magnetization on every tetrahedron and the ensemble of these configurations forms a macroscopically degenerate, but highly correlated, ground-state manifold. Such a collective state is termed a Coulomb phase because coarse-grained spin configurations within the manifold form a divergence free vector-field that implies dipolar correlations.[7–9] Experiments probing magnetic correlations, and hence the solenoidal field, should include sharp pinch point features as in related classical spin ice materials where ferromagnetic Ising interactions dominate.[10] Both classical spin ice and the classical Heisenberg antiferromagnet may be classified as Coulomb phases but, while there is much activity and progress in exploring quantum spin ice, much less is understood about the quantum limit of the Heisenberg model. There is theoretical evidence that pinch point correlations survive,[2,3,11–13] but the specific character of the ground state and of the magnetic excitations is unknown.

The experimental challenge lies in realizing the pyrochlore Heisenberg model in a real material. The highly degenerate manifold of the Coulomb phase is susceptible to small perturbations[2] and lattice instabilities[14] such that at low temperatures the spin liquid phase is more often than not supplanted by a broken symmetry phase. So far, the closest realizations of a Heisenberg antiferromagnet on a pyrochlore lattice have been found in the cubic-spinels. Many of these materials exhibit significant exchange interactions extending to the second and third nearest neighbours.[15] Magnetic frustration is manifest through self-organized independent hexagonal clusters,[16–19] but a magneto-structural transition severely impacts almost half of the magnetic bandwidth.

Extrinsic disorder, in the form of impurity ions, or variations in magnetic exchange interactions caused by chemical disorder may also disrupt the spin liquid. Generally, these perturbations result in a spin freezing transition at low temperatures.[20–22] For example, in the Heisenberg pyrochlore $Y_2Mo_2O_7$ weak disorder results in a fully frozen, disordered state, with isotropic short range spin correlations.[23,24] Here, we demonstrate that disorder is not necessarily fatal to the search for quantum spin liquids and can act to only freeze the lowest energy magnetic degrees of freedom. At higher energies a magnetic excitation continuum

characteristic of fractionalized excitations persists.

$NaCaNi_2F_7$ is one member of a family of recently discovered transition metal pyrochlore flourides where charge balance in the neutral chemical structure requires an equal mixture of Na^{1+} and Ca^{2+}.[25–27] Diffraction measurements probing the average crystal structure indicate that Na^{1+} and Ca^{2+} are uniformly and randomly distributed on the A-site of the pyrochlore lattice. Magnetic susceptibility measurements reveal Curie-Weiss behaviour, with an effective moment of $p_{eff} = 3.6(1)\ \mu_B$, consistent with $S = 1$, and a Curie-Weiss temperature of $\theta_{CW} = 129(1)$ K.[26] A spin-glass like freezing transition is observed at $T_f = 3.6$ K in DC and AC magnetic susceptibility measurements.[26] This freezing may result from the charge disorder that can be expected to generate a random variation in the magnetic exchange interactions. For the Heisenberg pyrochlore antiferromagnet described by the Hamiltonian $H = \sum_{ij} J_{ij}\mathbf{S}_i \cdot \mathbf{S}_j$ the freezing temperature provides an estimate of the strength of bond disorder $\delta J = \sqrt{3/8}k_B T_f = 0.19$ meV, for $S = 1$.[21]

Notwithstanding the glassy features of $NaCaNi_2F_7$, we will provide evidence that a quantum spin liquid (QSL) remains a very realistic possibility. First, the co-existence of a low energy frozen component and the intrinsic excitations of a QSL at higher energies is manifest in the magnetic specific heat $C_m(T)$. Second, we use theoretical tools including the self consistent Gaussian approximation and classical Monte Carlo to perform extensive fits to our neutron scattering data and determine the relevant Hamiltonian. We find that it is predominantly characterized by a Heisenberg model with small additional exchange terms. Third, the presence of a continuum of magnetic excitations coupled with the unusually large inelastic spectral weight suggest that this $S = 1$ magnet is in the strongly quantum regime. Finally, in the absence of a definitive theoretical understanding of the quantum version of the pyrochlore Heisenberg antiferromagnet, we explore several scenarios that may be consistent with our experimental findings.

Fig. 1a shows the magnetic specific heat $C_m(T)$. Beginning with the high temperature regime for $T > 18$ K, $C_m(T)$ very closely follows the form expected for the classical spin liquid – Villain's cooperative paramagnet – phase of the Heisenberg antiferromagnet on a pyrochlore lattice. Indeed, our classical Monte-Carlo simulation of the Heisenberg model, using exchange parameters extracted from analysis of inelastic neutron scattering measurements to be discussed below, aligns very closely with the data. In the second regime, where T is of the order of the Heisenberg coupling, $C_m(T)$ falls below the classical model and the

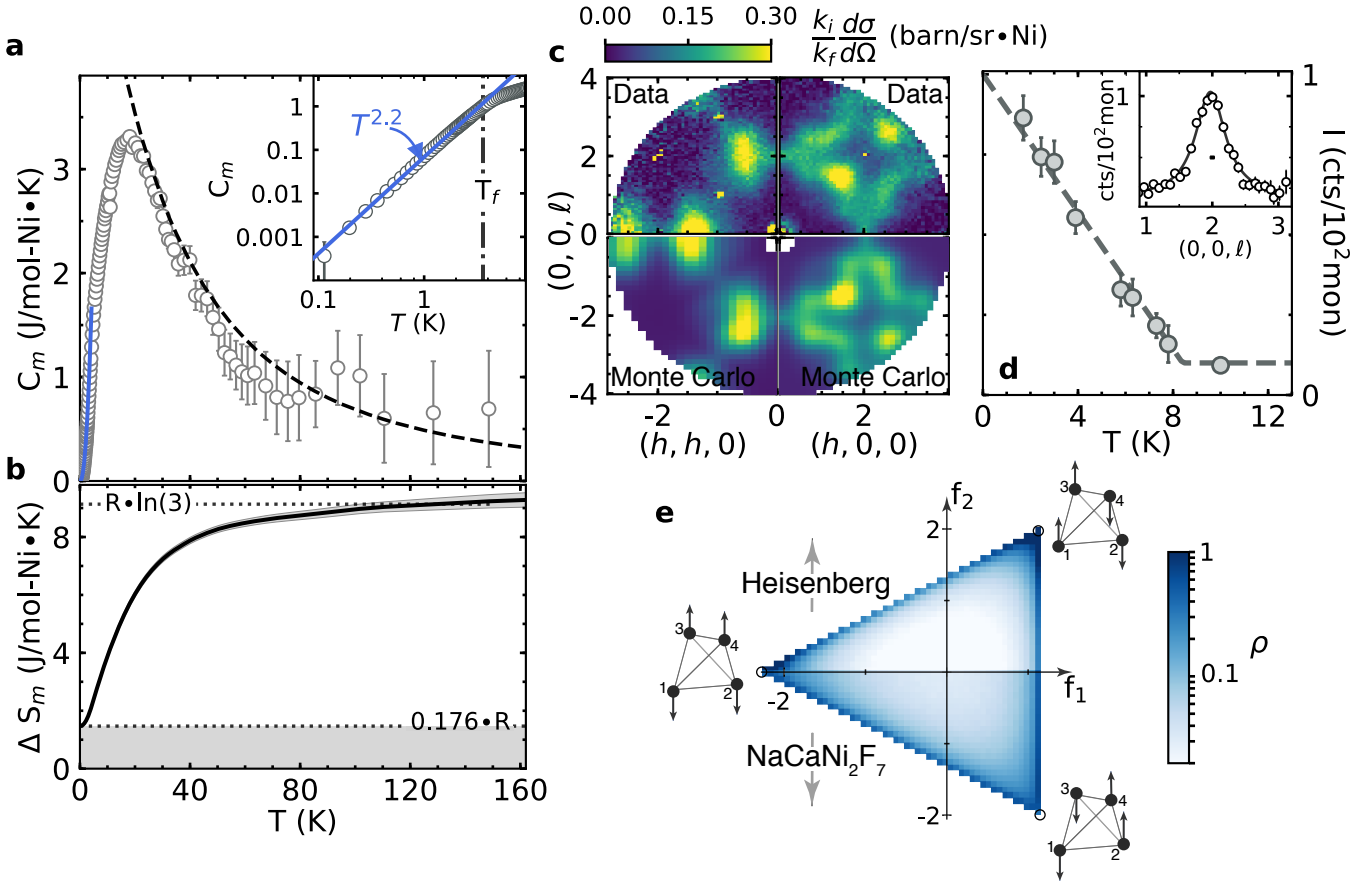

Figure 1: Spin freezing in $NaCaNi_2F_7$. **a**, Magnetic specific heat. Dashed line is a classical Monte-Carlo simulation. Solid line is a fit to $C_m(T) = AT^{\alpha}$, with $A = 0.07(1)$ and $\alpha = 2.2(1)$. Inset shows the low temperature region. **b**, Magnetic entropy obtained by integration of C/T between $T = 150$ K and 100 mK corresponding to 84% of $R\ln(3)$. **c**, Diffuse elastic ($E = 0$) magnetic scattering, integrated over the resolution window of ± 0.37 meV and obtained by subtracting $T = 40$ K data from that at 1.6 K. Lower quadrants display disorder and configuration averaged ground state Monte-Carlo structure factors. **d**, Temperature dependent intensity of the diffuse elastic scattering around $\mathbf{q} = (0, 0, 2)$, dashed line is $(1 - T/T_f)^{2\beta}$, with $T_f = 8.2$ K and $\beta = 0.5$. Inset shows the $T = 1.6$ K line shape across the pinch point, integrated over $-0.1 < (h, h, 0) < 0.1$, the horizontal dash denotes the instrumental resolution. Error bars in all figures represent one standard deviation. **e**, Histogram of bond vector order parameter components (f_1, f_2) from classical Monte-Carlo simulations for Heisenberg and exchange model relevant to $NaCaNi_2F_7$ including exchange disorder. Extremal spin configurations corresponding to collinear spin arrangements are shown.

broad maximum at 18 K signals the onset of a collective quantum state. Finally, a third distinct regime is identified below $T_f = 3.6$ K, where a discontinuity in the derivative of $C_m(T)$ occurs. The approximately quadratic power law T dependence below this anomaly is interpreted as a consequence of static, or frozen, magnetism below T_f.

$C_m \propto T^2$ for $T < T_f$ is characteristic of dense frustrated magnets where some disorder is present; the exponent appears to be independent of the dimensionality of the interacting system.[24,28,29] This quadratic temperature dependence generally indicates gapless, linearly dispersing modes in two dimensions or along nodal lines in momentum space. While the lack of translational symmetry implies these do not manifest as coherent modes in neutron scattering measurements, the corresponding density of states should be reflected there, albeit below the range of energies that we have accessed spectroscopically. The low temperature specific heat exponent of $\alpha = 2.2(1)$ could arise from the intrinsic low energy sector of a putative QSL. An alternative interpretation is attributed to the existence of Halperin Saslow spin waves, the normal modes of the frozen state,[30,31] although the presence of line nodes in the dispersion relation is non-trivial.

In Fig. 1b we show the magnetic entropy recovered between 100 mK and 150 K which saturates at 84% of the available $R\ln(3)$ for $S = 1$. We interpret the $0.176R$/spin residual entropy at 100 mK as indicating broken ergodicity. Specifically, we propose that below T_f, a metastable spin configuration within the Coulomb phase manifold is kinetically arrested by the disorder potential so the material no longer explores all states of a given energy. However, most of the magnetic entropy is associated with higher energy states. Thus, there is an energy scale above $k_B T_f$ where excitations are unaffected by exchange disorder and reflect the site averaged spin Hamiltonian of $NaCaNi_2F_7$. This notion is indeed verified through momentum and energy resolved neutron scattering measurements, which enable us to explicitly separate these two components of the spin correlation function. We first investigate the frozen component at low energies and then the high energy continuum of excitations.

Figure 1c shows the elastic neutron intensity in two high-symmetry reciprocal lattice planes of the cubic lattice. The elastic magnetic signal is dominated by extended diffuse intensity arising from short range correlated spin configurations that are static within the 10 ps time window of our measurement. Neutron intensity is concentrated in lobes centered on $(2n \pm 0.6, 2n \pm 0.6, 0)$ positions, where n is an integer. Near (002) and (220), where sharp

pinch point features representing long-range correlations of the pure Heisenberg model are expected, the momentum distribution of the scattering is broader than the experimental resolution. The inverse momentum width corresponds to a real-space correlation length of $\xi = 6$ Å, or just two nearest neighbour lattice spacings.

Figure 1d shows the onset of elastic scattering upon cooling below 8 K. This temperature is significantly higher than the 3.6 K T_f extracted from susceptibility measurements.[26] Inelastic neutron scattering probes the imaginary part of the magnetic susceptibility in the THz frequency range, a timescale orders of magnitude faster than AC susceptibility, and the upward shift in apparent freezing temperature with the characteristic measurement frequency indicates a glass-like transition. We find the momentum width of the elastic signal is independent of temperature indicating that spatial correlations are unaffected by the freezing transition. The observation of a time-scale dependent T_f, temperature independent spatial correlations, and residual entropy are consistent with kinetically arrested magnetism in $NaCaNi_2F_7$. Below T_f low energy spin configurations become trapped by the disorder potential, resulting in an out-of-equilibrium frozen configuration that is a snap-shot of the near degenerate manifold of states. Integrating the elastic ($E = 0$) intensity over momentum we find that the frozen moment accounts for only $|\langle \mathbf{S} \rangle| / S = 44\%$ of the saturation magnetization. Thus, magnetism in $NaCaNi_2F_7$ at $T = 1.6$ K is predominantly dynamic. Such a small fraction of frozen magnetization is comparable to two-dimensional frustrated magnets[32] but in three-dimensional magnets is unique to $NaCaNi_2F_7$.

To better understand the nature of the frozen low temperature state, we have carried out classical Monte-Carlo simulations of the Heisenberg Hamiltonian relevant to $NaCaNi_2F_7$. Random bond disorder was included by sampling from a box distribution, with a half width of $\delta J = 0.19$ meV and exchange parameters extracted from an independent analysis of inelastic neutron scattering data. In figure 1c we compare the measured elastic scattering with the corresponding numerically modeled signal. The high fidelity fit gives confidence in our optimized magnetic Hamiltonian. To gain additional insight we complement these results with a study of local metrics for individual tetrahedra on the pyrochlore lattice.

In the absence of disorder, the energy of the classical Heisenberg Hamiltonian is minimized by all states with zero total spin per tetrahedra, $\mathbf{S}_{\text{tot}} = \sum_{i=1}^{4} \mathbf{S}_i = 0$. We find the lowest energy states for the bond-disordered Heisenberg Hamiltonian with small anisotropic exchanges relevant to $NaCaNi_2F_7$ also fall within the $\mathbf{S}_{\text{tot}} = 0$ manifold [see supple-

mental information]. This manifold is parameterized by the order parameters $f_1 = [(\mathbf{S}_1+\mathbf{S}_2)\cdot(\mathbf{S}_3+\mathbf{S}_4)-2\mathbf{S}_1\cdot\mathbf{S}_2-2\mathbf{S}_3\cdot\mathbf{S}_4]/\sqrt{12}$ and $f_2=(\mathbf{S}_1\cdot\mathbf{S}_3+\mathbf{S}_2\cdot\mathbf{S}_4-\mathbf{S}_2\cdot\mathbf{S}_3-\mathbf{S}_1\cdot\mathbf{S}_4)/2$.[14,33] The statistical distribution of f_1 and f_2 over a Monte Carlo ensemble of tetrahedra provides a local characterization of the particular $\mathbf{S}_{\rm tot}=0$ spin configuration. Such histograms of (f_1, f_2) extracted from our Monte-Carlo simulations are shown in figure 1e where possible values span an equilateral triangle in the (f_1, f_2) plane. Tetrahedra with pairs of antiparallel spins lie along the triangular edges while collinear spin configurations are at the vertices. The classical Heisenberg (only) model with weak bond disorder is glassy[21] with a tendency to form locally collinear states; this is confirmed by the results in the top half of Fig. 1e.[20] The enhanced density along the boundaries, and away from the corners, of the lower part of the triangle in Fig.1e indicates the tendency to form configurations of pairwise collinear spins when additional small anisotropic interactions specific to $NaCaNi_2F_7$ are added.

In Fig. 2 we present the momentum and energy dependence of inelastic magnetic scattering for $NaCaNi_2F_7$. In contrast to the distinct maxima in the elastic scattering (Fig. 1), the dynamic structure factor forms a bow tie pattern with pinch points characteristic of dipolar spin correlations. The scattering closely resembles expectations for the Heisenberg antiferromagnet on the pyrochlore lattice[7,8,15] but with important deviations, including a slight momentum broadening and reduction of intensity around the pinch points. Magnetic scattering evolves into a continuum with a well-defined momentum structure at higher energies. The highest energy magnetic excitations are spread everywhere in momentum space except at the Γ point where neutron intensity is precluded for a Heisenberg model.

Fig. 3a shows the equal time structure factor $S(\mathbf{q})$ obtained from the energy integrated magnetic neutron scattering intensity. More detailed information is provided by polarized neutron scattering in the (h, h, ℓ) plane which is sensitive to spin components within the (h, h, ℓ) reciprocal lattice plane for the non-spin-flip (NSF) channel, and along $(1, -1, 0)$ for the spin-flip channel (SF). The similarity of SF and NSF magnetic neutron intensities in figure 3a is evidence of a near spin-space isotropic manifold and immediately rules out single ion-anisotropy terms. Weakly anisotropic interactions are revealed by two features of the polarized intensity. First, the SF scattering exhibits a pronounced asymmetry of the lobes of intensity centered on $(\pm0.6, \pm0.5, 2)$ positions about the dashed line parallel to $(1, 1, 0)$ and passing though $(0, 0, 2)$ indicated in figure 3b. Second, the NSF intensity is diminished around the $(0, 0, 2)$ pinch point positions.

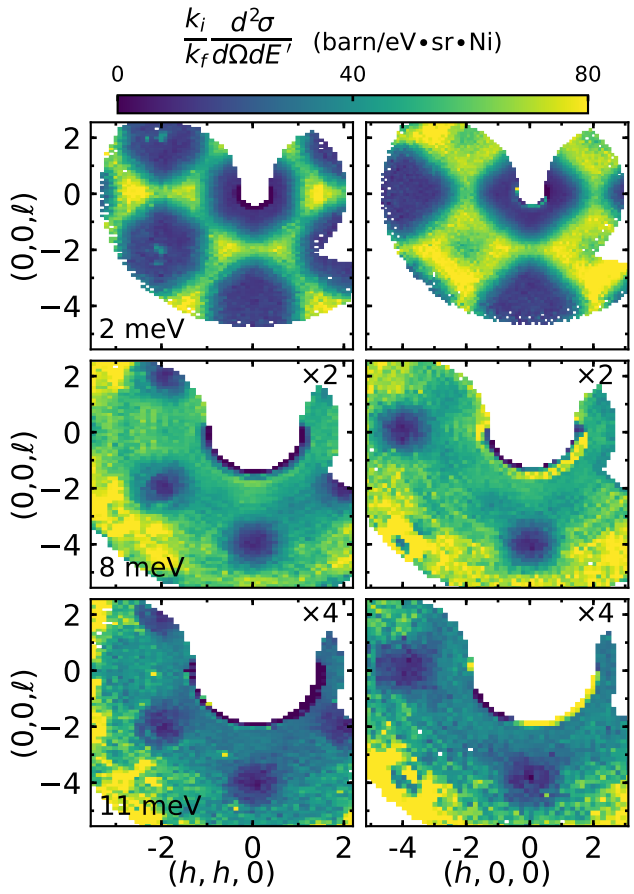

Figure 2: Separation of magnetic energy scales in $NaCaNi_2F_7$. Momentum and energy dependence of inelastic magnetic scattering in $NaCaNi_2F_7$ for the (h, h, ℓ) and $(h, k, 0)$ scattering planes at $T = 1.5$ K. Each slice was integrated over an energy transfer range of ± 0.25 meV. Above energy transfers of 0.5 meV the dynamic magnetic correlations form a "bow tie" pattern in momentum space. The sharp pinch point like features around $(2, 0, 0)$ and $(2, 2, 0)$ positions indicate that the net magnetisation per tetrahedron vanish in the Coulomb phase. Above energies of 5 meV the scattering forms a broad continuum with no intensity around the Γ points.

We have analyzed the energy integrated neutron spectra using a self-consistent Gaussian approximation (SCGA) for the equal time structure factor[15] using the full symmetry allowed nearest-neighbour Hamiltonian $H = 1/2 \sum_{ij} J_{ij}^{\mu\nu} S_i^\mu S_j^\nu$, where the 3×3 interaction matrix $J^{\mu\nu}$ is parameterized by four independent terms: J_1, J_2, J_3, and J_4,[34] in additional to next nearest neighbour Heisenberg exchange J_{NNN}. A symmetry allowed biquadratic exchange

term was not included in our analysis. We find the best global fit of the measured equal time factor with the SCGA using the exchange parameters: $J_1 = J_2 = 3.2(1)$ meV, $J_3 = 0.019(3)$ meV $J_4 = -0.070(4)$ meV, and $J_{NNN} = -0.025(5)$ meV. This set of parameters yields a Curie Weiss temperature $\tilde{\Theta}_{\rm CW} = -150$ K which may be compared with the experimentally determined value of $\Theta_{\rm CW} = -129(1)$ K.[26] Details of the fitting procedure are contained in the supplementary information and the resulting modeled neutron intensity is shown in figure 3b. Although the SCGA is an approximate procedure, we find exceptional agreement between the model and data. Furthermore, these exchange parameters were directly input into the classical Monte-Carlo simulations which builds further confidence in the SCGA. Thus, the spin Hamiltonian for $NaCaNi_2F_7$ very closely approximates the $S = 1$ Heisenberg antiferromagnet on the pyrochlore lattice, perturbed by small symmetric and antisymmetric exchange anisotropies as well as next nearest neighbour interactions.

A number of theoretical investigations have shown that small perturbations in the classical Heisenberg model, J', in the form of exchange anisotropies or further neighbour interactions, result in a magnetically ordered phase below temperatures of the order $J'S^2$.[2,15,33,36,37] In $NaCaNi_2F_7$ these perturbations are significantly smaller than the freezing temperature, such that any lower temperature transition is pre-empted by spin freezing and inaccessible to experiment. Indeed, our classical Monte-Carlo simulations for the anisotropic Hamiltonian relevant to $NaCaNi_2F_7$, but in the absence of exchange disorder, do not indicate long-range ordering above $T = 500$ mK. This temperature is well below the broad maximum in specific heat where quantum mechanical fluctuations become important and our classical simulations are no longer strictly valid.

In figure 4 we present the momentum and energy resolved spin-flip neutron scattering cross-section. For our experiment this cross-section is sensitive to magnetic scattering and nuclear incoherent scattering, thus data in Fig. 4 are representative of the dynamic structure factor uncontaminated by coherent non-magnetic scattering. The magnetic excitations form a continuum that extends over an energy bandwidth of $\sim$12.5 meV$\sim 4J_1S$. Along the $(h, h, 2)$ direction, transverse to the pinch points,[8] the inelastic neutron intensity is relatively featureless. However, along the (2,2,ℓ) direction, longitudinal to the pinch points, the magnetic scattering is more structured and, importantly, does not factorize as found theoretically for the classical limit of the Heisenberg model on the pyrochlore lattice.[38] In the constant momentum and energy transfer cuts plotted in Fig. 4 b and c very broad dis-

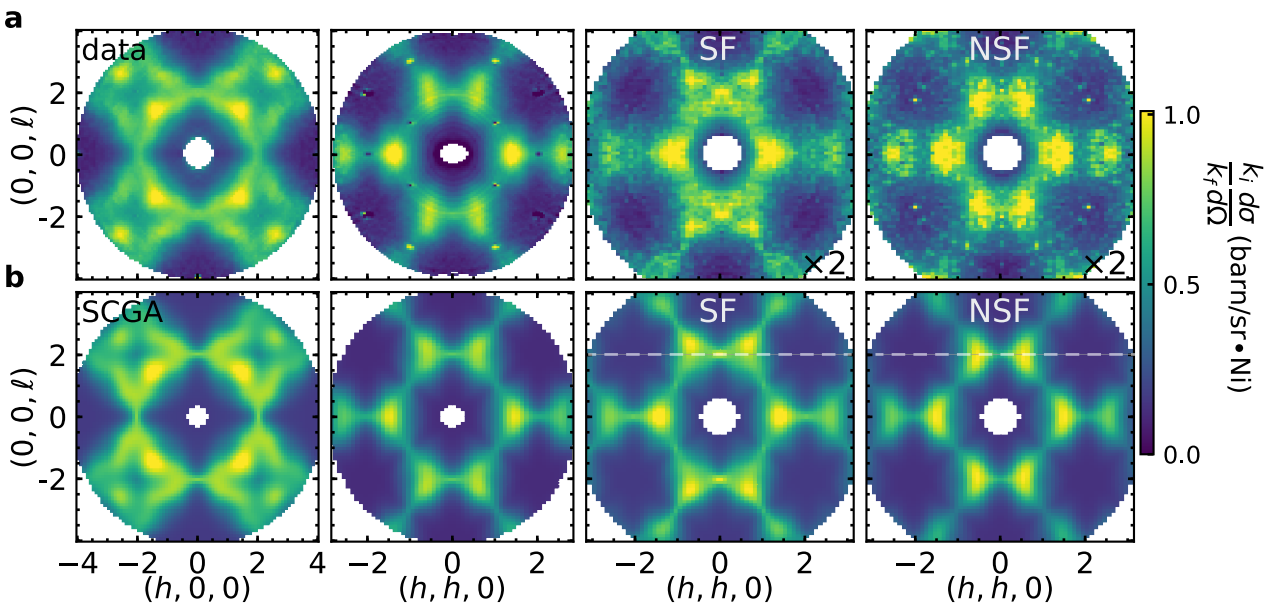

Figure 3: Equal time structure factor in $NaCaNi_2F_7$. **a**, Measured neutron cross-section integrated over the range $0 < E < 14$ meV. Polarized neutron measurements are labelled by SF, which measures components of the dynamic spin correlation function that are perpendicular to the (h, h, ℓ) scattering plane, and NSF, which measures the component of the dynamics spin correlation function polarized within the (h, h, ℓ) scattering plane and perpendicular to momentum transfer. **b**, Energy integrated neutron cross-section calculated using the self-consistent Gaussian approximation (SCGA) and exchange parameters $J_1 = J_2 = 3.2(1)$ meV, $J_3 = 0.019(3)$ meV $J_4 = -0.070(4)$ meV, $J_{NNN} = -0.025(5)$ meV. Dashed lines delineate plane of asymmetry in the SF scattering. The dipole approximation for the Ni^{2+} magnetic form factor[35] was used when converting the calculated $\mathcal{S}(\mathbf{q})$ to a neutron cross-section.

persive ridges are observed that are reminiscent of heavily damped spin-waves. While the spectrum is gapless down to the 0.17 meV scale set by our finest energy resolution measurements, the dynamic structure factor is peaked at finite energy transfers and can be fit with the spectral form of an over-damped harmonic oscillator. The characteristic energy scale disperses from $E_q = 4.8$ meV$\sim J$ at the pinch point $\mathbf{q} = (2, 2, 0)$, to $E_q = 7.8$ meV at the nodal point $\mathbf{q} = (2, 2, 1)$. This spectrum distinguishes $NaCaNi_2F_7$ from recent theoretical treatments of the semi-classical Heisenberg model which find a purely diffusive response at

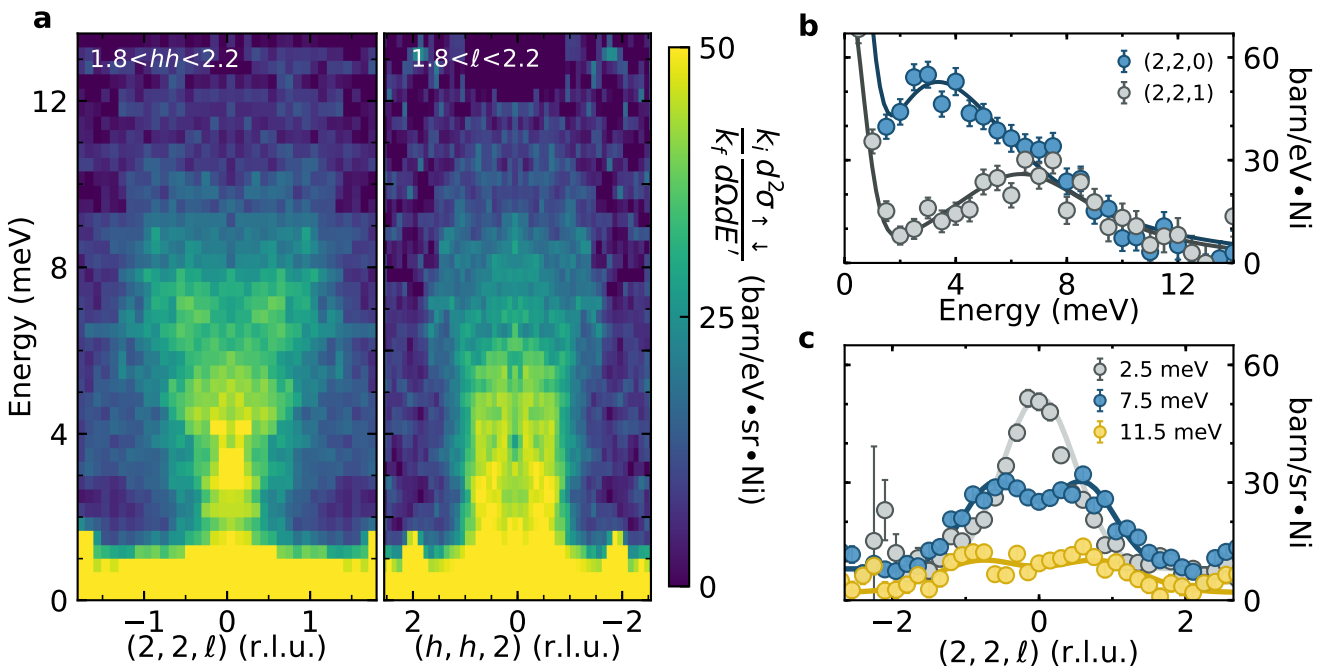

Figure 4: Magnetic excitations in $NaCaNi_2F_7$. **a**, Energy-momentum cuts through the spin-flip portion of the polarized neutron scattering cross-section at $T = 1.6$ K. **b**, Constant momentum cuts of the spin-flip cross-section through a pinch point at $\mathbf{q} = (2, 2, 0)$ and nodal point at (2,2,1) integrated over $\ell \pm 0.2$. Solid lines are a fit to the sum of a Lorentzian function centered on the elastic line and a damped oscillator form $S(E) = \frac{(n+1)2\Gamma E}{\left(E^2 - E_q^2\right)^2 + (2\Gamma E)^2}$ where n is the thermal population factor, Γ a relaxation rate, and E_q the characteristic energy scale. **c**, Constant energy transfer cuts, integrated over $E \pm 0.25$ meV, showing the energy evolution of momentum dependent scattering which bifurcates above 5 meV and precludes a simple factorization of the dynamic structure factor as $S(\mathbf{q}, \omega) = S(\mathbf{q}) f(\omega)$.

the pinch points[13]. The absence of inelastic scattering at the Γ point and our polarized neutron measurements rule out any sizable single-ion anisotropies that could explain the peak in spectral weight at non-zero energy transfers. The only energy scale large enough to account for the resonance is the exchange interaction J_1.

Disorder in $NaCaNi_2F_7$ is small such that its effect is only to rearrange the low energy part of the spectrum for $E < k_B T_f$ and the underlying translational invariance of the Heisenberg spin Hamiltonian can be expected to prevail. Indeed, we find that $NaCaNi_2F_7$ forms a Coulomb-like phase, with $\mathbf{S}_{\text{tot}} \approx 0$ for every tetrahedron. The high energy excitations

correspond to propagating defects that violate this condition, and our observation of an excitation continuum means that such defects in the Heisenberg model cannot propagate as coherent quasiparticles carrying an angular momentum of $\hbar$.

A conservative interpretation is that the dispersing modes are overdamped spin waves of an underlying classical magnetic order, disrupted in $NaCaNi_2F_7$ by exchange disorder. Since the frozen spin configurations feature non-collinear interacting spins, single particle $S=1$ magnon excitations can decay from interactions with multimagnon states to form a continuum of scattering.[39] Such a scenario may be appropriate for the related pyrochlore XY antiferromagnet $NaCaCo_2F_7$.[25] Elastic magnetic neutron scattering from $NaCaCo_2F_7$ resembles that of an ordered antiferromagnet, consistent with the non-collinear magnetic structure favoured by an order-by-disorder mechanism.[40] This order develops at a temperature coincident with a broad peak in the magnetic specific heat, which constitutes the total magnetic entropy of the $J=1/2$ magnetic moments formed by Co ions. Furthermore, the fraction of elastic magnetic neutron intensity is 0.3(1),[40] almost exactly as expected for an ordered $S=1/2$ magnet ($S^2/S(S+1)=1/3$). Thus, it appears that in $NaCaCo_2F_7$ exchange disorder truncates the magnetic correlations of the classical antiferromagnetic order favoured by the underling Hamiltonian. This is distinct from the Heisenberg Hamiltonian we infer for $NaCaNi_2F_7$. It does not favour a magnetically ordered state, consistent with the magnetic specific heat and the strong inelastic magnetic neutron scattering.

In contrast to its Co counterpart, $NaCaNi_2F_7$ does not show a full recovery of the fraction of elastic magnetic neutron intensity; rather, the significant proportion of inelastic spectral weight suggests a quantum fluctuating state. For a QSL the magnetic spectral weight at $T=0$ must be entirely accounted for by the excitations and there can be no truly elastic scattering. For a semi-classical state the elastic scattering should carry a fraction of $S^2/S(S+1)$ of the spectral weight, which for $S=1$ equals $1/2$. By integrating the measured dynamic spin correlation function $S(\mathbf{q},E)$ over momentum and energy, including the elastic diffuse magnetic scattering, we recover the total spectral weight of $3\int \mathcal{S}(\mathbf{q},E)\,dEd^3q = 13(1)$, which is consistent with the $(3.7)^2 = 13.7\ \mu_B^2$ effective moment extracted from the magnetic susceptibility.[26] Comparing the spectral weight for elastic, $E<0.7$ meV, and inelastic scattering, $0.7<E<14$ meV, we find $\sim$90% of the magnetic scattering is inelastic in the low T limit. This significantly exceeds the 50% mark for a semi-classical ground state and is direct evidence of a spin system dominated by quantum fluctuations.

Our experimental and theoretical results admit the possibility that $NaCaNi_2F_7$ is a QSL driven to freezing by weak exchange disorder. At energies above $E = k_b T_f$ the continuous spectrum indicates the absence of coherent quasiparticles carrying angular momentum $\hbar$ and is consistent with the fractionalization of a spin flip excitation into weakly interacting quasiparticles with angular momentum $\hbar/2$. The fact that the residual entropy as a fraction of the total spin entropy ($\Delta S/R\ln(3) = 16(4)\%$) is within error bars of the fraction of the total spectral weight contained in elastic scattering ($\langle m_{elastic}\rangle^2/g^2S(S+1)) = 10(2)\%$) indicates the exchange disorder associated with the mixed Na/Ca site induces a non-ergodic low energy landscape for these quasiparticles. Such a separation of energy scales between frozen and fluctuating components is observed in other materials that support QSLs. For example in the one-dimensional $S = 1/2$ chain $KCuF_3$, the spinon continuum is observable at high energies even in the Néel ordered state.[41]

A QSL remains a realistic contender for the ground state of $NaCaNi_2F_7$, but preciously little is known theoretically about the $S = 1$ Heisenberg model on the pyrochlore lattice. Our finding that, at the classical level, the frozen state involves tetrahedra with quasi-static anti-parallel pairs of spins at low temperatures points to a quantum scenario where these pairs correspond to a singlet covering of the pyrochlore lattice. Since there are exponentially many such coverings, effects analogous to those studied extensively for dimer models may play a role in explaining the specific value of the residual entropy.[12] In addition, the $S = 1$ Heisenberg model admits other rich possibilities. One such picture that might be pursued involves fluctuating Haldane/AKLT loops decorating the pyrochlore lattice.[42] In the AKLT construction, each $S = 1$ degree of freedom is built from two $S = 1/2$ objects and the collective quantum state is projected to the $S = 1$ subspace. Loops are constructed by joining neighbouring spins into singlets across each bond. A single spin flip excitation will break this bond, fracturing the loop and leaving a chain with two free $S = 1/2$, one at each end. These end states may then act as bulk fractionalized excitations that are deconfined within the quantum superposition of fluctuating loop coverings.[43] In the absence of any significant lattice distortion or cluster formation, such liquid like states remain a realistic possibility on the pyrochlore lattice and could help to understand our observation of residual entropy and continuum scattering in $NaCaNi_2F_7$.

METHODS

The identification of any commercial product or trade name does not imply endorsement or recommendation by the National Institute of Standards and Technology.

Specific Heat. Heat capacity measurements were conducted using a Quantum Design PPMS with a dilution insert for temperatures between 100 mK and 4 K, and standard insert for temperatures between 2 K and 270 K. All measurements were carried out on the same 5 mg single crystal using the adiabatic pulse method. The non-magnetic contribution was determined by scaling the measured specific heat of the iso-structural compound $NaCaZn_2F_7$ by the relative Debye temperatures.

Neutron Scattering. All neutron scattering measurements were performed on the same 3 g single crystal, grown as described elsewhere.[26] Unpolarized neutron scattering measurements were preformed on the MACS spectrometer[44] at the NIST Center for Neutron Research. The neutron momentum transfer is indexed using the Miller indices of the cubic unit cell, $(h, k, \ell) = (2\pi/a, 2\pi/a, 2\pi/a)$, where $a = 10.31$ Å. Measurements were conducted with the sample oriented in both the (h, h, ℓ) and $(h, k, 0)$ scattering planes. Elastic ($E = 0$) measurements were conducted with the monochromator in a vertical focusing configuration using a neutron energy of 5 meV. Two configurations were utilized for inelastic measurements, both with the monochromator in double focusing mode. For energy transfers below 1.4 meV, MACS was operated with fixed final energy of 3.7 meV and Be BeO filters before and after the sample respectively. For energy transfers above 1.4 meV we used a fixed final energy of 5 meV with a Be filter after the sample and no incident beam filter. The data for energy transfers above 1.4 meV was corrected for contamination from high-order harmonics in the incident beam neutron monitor.

Polarized neutron scattering measurements were carried out on the HYSPEC spectrometer[45] at the Spallation neutron Source at Oak Ridge National Lab. An incident neutron energy of 17 meV was selected using a Fermi chopper rotating at 240 Hz resulting in an energy resolution of $\delta E = 1.4$ meV on the elastic line. The incident neutron beam polarization was defined using a vertically focusing Heusler monochromator while the outgoing beam polarization was selected using a radially collimating supermirror array. All polarized measurements were conducted with the guide field applied perpendicular to the (h, h, l) scattering plane, along the $(1, -1, 0)$ direction. In this configuration, spin-flip scattering measures the component

of magnetic cross section that is polarized within the scattering plane, while non-spin-flip measures the out-of-plane component. The flipping ratio measured on a $(4, 4, 0)$ nuclear Bragg peak was 16. All data reduction and analysis was carried out using the Mantid software suite.[46]

Measured neutron count rates from both instruments were placed into absolute units of the neutron scattering cross-section using incoherent elastic scattering from the sample. The scale factor for conversion to absolute units was additionally cross-checked against measurements from a Vanadium standard.

Numerical Methods. We fit the static structure factor from the neutron scattering data to the corresponding prediction of the self-consistent Gaussian approximation (SCGA) at 1.6 K, to obtain the parameter set in the main text. Details of the method, including the cost function and error analysis are discussed in the supplementary information. The results of the SCGA are complemented by classical Monte-Carlo (MC) calculations, for both the specific heat and the structure factor. MC simulations used single spin updates for continuous spin on pyrochlore lattices (with 16 site cubic unit cells) of size $N = 16L^3$ for $L = 3$ to $L = 10$. For determining the classical ground state of the fitted spin Hamiltonian, parallel tempering MC[47] was carried out with $T_{min} = 0.01$ K and $T_{max} = 1$ K with the number of replicas $N_r = \sqrt{N} \ln\left(T_{max}/T_{min}\right)$ (approximately 100 for $L = 3$ and 400 for $L = 8$, the two sizes studied extensively, see supplementary for more analyses) and the simulation carried out for 10^8 total steps. With the lowest energy configurations encountered in this finite Monte-Carlo run, further iterative minimization was performed to accelerate the approach to the classical ground state. For these optimized spin configurations (many of which are local minima) two-component local order parameters (f_1 and f_2) are calculated on all $N/4$ tetrahedra of a fixed orientation ("up"). This is repeated for 50 – 100 bond-disorder realizations and the combined data set, including all tetrahedra and disorder realizations, is used to obtain the 2D histogram in Fig. 1. The static structure factor from these low energy zero temperature configurations, for $L = 8$, was averaged to obtain an estimate of the elastic cross-section. Further details of all methods and algorithms employed are discussed in the supplementary information.

ACKNOWLEDGMENTS

We are grateful to Yuan Wan for enlightening discussions. This work benefited from many insightfull comments from Oleg Tchernyshyov. We would also like to thank Roderich Moessner, John Chalker, and Senthil Todadri for critical reading of this manuscript. Work at the Institute for Quantum Matter was supported by the U.S. Department of Energy, Office of Basic Energy Sciences, Division of Material Sciences and Engineering under grant DE-FG02-08ER46544. Access to MACS was provided by the Center for High Resolution Neutron Scattering, a partnership between the National Institute of Standards and Technology and the National Science Foundation under Agreement No. DMR-1508249. A portion of this research used resources at the Spallation/ Neutron Source, a DOE Office of Science User Facility operated by the Oak Ridge National Laboratory. This work was supported by the Paul Scherrer Institut by providing the supermirror analyzer as a temporary loan to Oak Ridge National Laboratory. We gratefully acknowledge the Johns Hopkins Homewood High Performance Cluster (HHPC) and the Maryland Advanced Research Computing Center (MARCC), funded by the State of Maryland, for computing resources.

AUTHOR CONTRIBUTIONS

K. W. P., A. S., B. W., J. A. R., and Y. Q. performed the neutron scattering experiments. K. W. P. performed the specific heat measurements and analyzed the experimental data. J. W. K. and R. J. C. synthesized and characterized the single crystal sample. H. J. C and S. Z. performed Monte-Carlo simulations and self consistent Gaussian approximation calculations, along with assisting with the theoretical interpretation. K. W. P. wrote the manuscript with input from all co-authors. C. L. B. oversaw all aspects of the project.

---

[1] Jacques Villain, "Insulating spin glasses," Zeitschrift für Physik B Condensed Matter **33**, 31–42 (1979).

[2] A. B. Harris, A. J. Berlinsky, and C. Bruder, "Ordering by quantum fluctuations in a strongly frustrated Heisenberg antiferromagnet," Journal of Applied Physics **69**, 5200–5202 (1991).

[3] B. Canals and C. Lacroix, "Pyrochlore antiferromagnet: A three-dimensional quantum spin liquid," Phys. Rev. Lett. **80**, 2933–2936 (1998).

[4] Benjamin Canals and Claudine Lacroix, "Quantum spin liquid: The Heisenberg antiferromagnet on the three-dimensional pyrochlore lattice," Phys. Rev. B **61**, 1149–1159 (2000).

[5] R. Moessner and J. T. Chalker, "Properties of a classical spin liquid: The Heisenberg pyrochlore antiferromagnet," Phys. Rev. Lett. **80**, 2929–2932 (1998).

[6] R. Moessner and J. T. Chalker, "Low-temperature properties of classical geometrically frustrated antiferromagnets," Phys. Rev. B **58**, 12049–12062 (1998).

[7] S. V. Isakov, K. Gregor, R. Moessner, and S. L. Sondhi, "Dipolar spin correlations in classical pyrochlore magnets," Phys. Rev. Lett. **93**, 167204 (2004).

[8] C. L. Henley, "Power-law spin correlations in pyrochlore antiferromagnets," Phys. Rev. B **71**, 014424 (2005).

[9] Christopher L. Henley, "The Coulomb phase in frustrated systems," Annual Review of Condensed Matter Physics **1**, 179–210 (2010).

[10] T. Fennell, P. P. Deen, A. R. Wildes, K. Schmalzl, D. Prabhakaran, A. T. Boothroyd, R. J. Aldus, D. F. McMorrow, and S. T. Bramwell, "Magnetic Coulomb phase in the spin ice $Ho_2Ti_2O_7$," Science **326**, 415–417 (2009).

[11] Makoto Isoda and Shigeyoshi Mori, "Valence-bond crystal and anisotropic excitation spectrum on 3-dimensionally frustrated pyrochlore," J. Phys. Soc. Japan **67**, 4022–4025 (1998).

[12] R. Moessner, S. L. Sondhi, and M. O. Goerbig, "Quantum dimer models and effective hamiltonians on the pyrochlore lattice," Phys. Rev. B **73**, 094430 (2006).

[13] Yuan Huang, Kun Chen, Youjin Deng, Nikolay Prokof'ev, and Boris Svistunov, "Spin-ice state of the quantum Heisenberg antiferromagnet on the pyrochlore lattice," Phys. Rev. Lett. **116**, 177203 (2016).

[14] Oleg Tchernyshyov, R. Moessner, and S. L. Sondhi, "Order by distortion and string modes in pyrochlore antiferromagnets," Phys. Rev. Lett. **88**, 067203 (2002).

[15] P. H. Conlon and J. T. Chalker, "Absent pinch points and emergent clusters: Further neighbor interactions in the pyrochlore Heisenberg antiferromagnet," Phys. Rev. B **81**, 224413 (2010).

[16] S.-H Lee, C. Broholm, W. Ratcliff, G. Gasparociv, Q. Huang, T. H. Kim, and S. W. Cheong, "Emergent excitations in a geometrically frustrated magnet," Nat. **418**, 856–858 (2002).

[17] K. Kamazawa, S. Park, S.-H. Lee, T. J. Sato, and Y. Tsunoda, "Dissociation of spin objects in geometrically frustrated $CdFe_2O_4$," Phys. Rev. B **70**, 024418 (2004).

[18] J.-H. Chung, M. Matsuda, S.-H. Lee, K. Kakurai, H. Ueda, T. J. Sato, H. Takagi, K.-P. Hong, and S. Park, "Statics and dynamics of incommensurate spin order in a geometrically frustrated antiferromagnet $CdCr_2O_4$," Phys. Rev. Lett. **95**, 247204 (2005).

[19] K. Tomiyasu, H. Suzuki, M. Toki, S. Itoh, M. Matsuura, N. Aso, and K. Yamada, "Molecular spin resonance in the geometrically frustrated magnet $MgCr_2O_4$ by inelastic neutron scattering," Phys. Rev. Lett. **101**, 177401 (2008).

[20] L Bellier-Castella, M JP Gingras, P CW Holdsworth, and R Moessner, "Frustrated order by disorder: The pyrochlore anti-ferromagnet with bond disorder," Canadian Journal of Physics **79**, 1365–1371 (2001).

[21] T. E. Saunders and J. T. Chalker, "Spin freezing in geometrically frustrated antiferromagnets with weak disorder," Phys. Rev. Lett. **98**, 157201 (2007).

[22] Arnab Sen and R. Moessner, "Topological spin glass in diluted spin ice," Phys. Rev. Lett. **114**, 247207 (2015).

[23] J. S. Gardner, B. D. Gaulin, S.-H. Lee, C. Broholm, N. P. Raju, and J. E. Greedan, "Glassy statics and dynamics in the chemically ordered pyrochlore antiferromagnet $Y_2Mo_2O_7$," Phys. Rev. Lett. **83**, 211–214 (1999).

[24] H. J. Silverstein, K. Fritsch, F. Flicker, A. M. Hallas, J. S. Gardner, Y. Qiu, G. Ehlers, A. T. Savici, Z. Yamani, K. A. Ross, B. D. Gaulin, M. J. P. Gingras, J. A. M. Paddison, K. Foyevtsova, R. Valenti, F. Hawthorne, C. R. Wiebe, and H. D. Zhou, "Liquidlike correlations in single-crystalline $Y_2Mo_2O_7$: An unconventional spin glass," Phys. Rev. B **89**, 054433 (2014).

[25] J. W. Krizan and R. J. Cava, "$NaCaCo_2F_7$: A single-crystal high-temperature pyrochlore antiferromagnet," Phys. Rev. B **89**, 214401 (2014).

[26] J. W. Krizan and R. J. Cava, "$NaCaNi_2F_7$: A frustrated high-temperature pyrochlore antiferromagnet with S=1 Ni^{2+}," Phys. Rev. B **92**, 014406 (2015).

[27] M. B. Sanders, J. W. Krizan, K. W. Plumb, T. M. McQueen, and Cava R. J., "$NaSrMn_2F_7$, $NaCaFe_2F_7$, and $NaSrFe_2F_7$: novel single crystal pyrochlore antiferromagnets," J. of Phys. Cond. Matter **29**, 045801 (2017).

[28] A. P. Ramirez, B. Hessen, and M. Winklemann, "Entropy balance and evidence for local spin singlets in a kagomé-like magnet," Phys. Rev. Lett. **84**, 2957–2960 (2000).

[29] Satoru Nakatsuji, Yusuke Nambu, Hiroshi Tonomura, Osamu Sakai, Seth Jonas, Collin Broholm, Hirokazu Tsunetsugu, Yiming Qiu, and Yoshiteru Maeno, "Spin disorder on a triangular lattice," Science **309**, 1697–1700 (2005).

[30] B. I. Halperin and W. M. Saslow, "Hydrodynamic theory of spin waves in spin glasses and other systems with noncollinear spin orientations," Phys. Rev. B **16**, 2154–2162 (1977).

[31] Daniel Podolsky and Yong Baek Kim, "Halperin-saslow modes as the origin of the low-temperature anomaly in $NiGa_2S_4$," Phys. Rev. B **79**, 140402 (2009).

[32] S.-H. Lee, C. Broholm, M. F. Collins, L. Heller, A. P. Ramirez, Ch. Kloc, E. Bucher, R. W. Erwin, and N. Lacevic, "Less than 50% sublattice polarization in an insulating $s = \frac{3}{2}$ kagomé antiferromagnet at $T \approx 0$," Phys. Rev. B **56**, 8091–8097 (1997).

[33] Gia-Wei Chern, R. Moessner, and O. Tchernyshyov, "Partial order from disorder in a classical pyrochlore antiferromagnet," Phys. Rev. B **78**, 144418 (2008).

[34] Kate A. Ross, Lucile Savary, Bruce D. Gaulin, and Leon Balents, "Quantum excitations in quantum spin ice," Phys. Rev. X **1**, 021002 (2011).

[35] P. J. Brown, *International Tables for Crystallography*, Vol. C (Springer, Berlin, 2006) Chap. 4.4.5, pp. 454–461.

[36] J. N. Reimers, A. J. Berlinsky, and A.-C. Shi, "Mean-field approach to magnetic ordering in highly frustrated pyrochlores," Phys. Rev. B **43**, 865–878 (1991).

[37] Maged Elhajal, Benjamin Canals, Raimon Sunyer, and Claudine Lacroix, "Ordering in the pyrochlore antiferromagnet due to Dzyaloshinsky-Moriya interactions," Phys. Rev. B **71**, 094420 (2005).

[38] P. H. Conlon and J. T. Chalker, "Spin dynamics in pyrochlore Heisenberg antiferromagnets," Phys. Rev. Lett. **102**, 237206 (2009).

[39] M. E. Zhitomirsky and A. L. Chernyshev, "Colloquium: Spontaneous magnon decays," Rev. Mod. Phys. **85**, 219–242 (2013).

[40] K. A. Ross, J. W. Krizan, J. A. Rodriguez-Rivera, R. J. Cava, and C. L. Broholm, "Static and dynamic xy-like short-range order in a frustrated magnet with exchange disorder," Phys. Rev. B **93**, 014433 (2016).

[41] Bella Lake, D. Alan Tennant, Chris D. Frost, and Stephen E. Nagler, "Quantum criticality and universal scaling of a quantum antiferromagnet," Nat Mater **4**, 329–334 (2005).

[42] Chong Wang, Adam Nahum, and T. Senthil, "Topological paramagnetism in frustrated spin-1 mott insulators," Phys. Rev. B **91**, 195131 (2015).

[43] Lucile Savary, "Quantum loop states in spin-orbital models on the honeycomb lattice," ArXiv e-prints (2015), arXiv:1511.01505 [cond-mat.str-el].

[44] J. A. Rodriguez, D. M. Adler, P. C. Brand, C. Broholm, J. C. Cook, C. Brocker, R. Hammond, Z. Huang, P. Hundertmark, J. W. Lynn, N. C. Maliszewskyj, J. Moyer, J. Orndorff, D. Pierce, T. D. Pike, G. Scharfstein, S. A. Smee, and R. Vilaseca, "MACS a new high intensity cold neutron spectrometer at NIST," Measurement Science and Technology **19**, 034023 (2008).

[45] Igor A Zaliznyak, Andrei T. Savici, V. Ovidiu Garlea, Barry Winn, Uwe Filges, John Schneeloch, John M. Tranquada, Genda Gu, Aifeng Wang, and Cedomir Petrovic, "Polarized neutron scattering on HYSPEC: the hybrid spectrometer at SNS," Journal of Physics: Conference Series **862**, 012030 (2017).

[46] O. Arnold, J.C. Bilheux, J.M. Borreguero, A. Buts, S.I. Campbell, L. Chapon, M. Doucet, N. Draper, R. Ferraz Leal, M.A. Gigg, V.E. Lynch, A. Markvardsen, D.J. Mikkelson, R.L. Mikkelson, R. Miller, K. Palmen, P. Parker, G. Passos, T.G. Perring, P.F. Peterson, S. Ren, M.A. Reuter, A.T. Savici, J.W. Taylor, R.J. Taylor, R. Tolchenov, W. Zhou, and J. Zikovsky, "Mantid data analysis and visualization package for neutron scattering and μSR experiments," Nucl. Instr. Meth. Phys. Res. Section A: Accelerators, Spectrometers, Detectors and Associated Equipment **764**, 156 – 166 (2014).

[47] Koji Hukushima and Koji Nemoto, "Exchange monte carlo method and application to spin glass simulations," Journal of the Physical Society of Japan **65**, 1604–1608 (1996).